Evolution on the biophysical fitness landscape of an RNA virus

Assaf Rotem[1,#], Adrian W.R. Serohijos[2,10,#], Connie B. Chang[1,9], Joshua T. Wolfe[3], Audrey E. Fischer[3], Thomas S. Mehoke[3], Huidan Zhang[1,4], Ye Tao[1], W. Lloyd Ung[1], Jeong-Mo Choi[2], João V. Rodrigues[2], Abimbola O. Kolawole[5], Stephan A. Koehler[1], Susan Wu[3], Peter M. Thielen[3], Naiwen Cui[1], Plamen A. Demirev[3], Nicholas S. Giacobbi[6], Timothy R. Julian[7,12], Kellogg Schwab[7], Jeffrey S. Lin[3], Thomas J. Smith[8], James M. Pipas[6], Christiane E. Wobus[5], Andrew B. Feldman[11], David A. Weitz[1,*], and Eugene I. Shakhnovich[2,*]

[1] School of Engineering and Applied Sciences and Department of Physics, Harvard University, 9 Oxford Street, Cambridge, MA 02138, USA
[2] Department of Chemistry and Chemical Biology, Harvard University, 12 Oxford Street, Cambridge, MA 02138, USA
[3] Johns Hopkins University Applied Physics Laboratory, 11100 Johns Hopkins Road, Laurel, MD 20723, USA
[4] Department of Cell Biology, Key Laboratory of Cell Biology, Ministry of Public Health, and Key Laboratory of Medical Cell Biology, Ministry of Education, China Medical University, Shenyang 110001, China
[5] Department of Microbiology and Immunology, University of Michigan Medical School, 1150 West Medical Center Drive, Ann Arbor, MI 48109, USA
[6] Department of Biological Sciences, University of Pittsburgh, 4249 Fifth Avenue, Pittsburgh, PA 15260, USA.
[7] Environmental Health Sciences and the Hopkins Water Institute, Johns Hopkins Bloomberg School of Public Health, Baltimore, Maryland 21231, USA
[8] Department of Biochemistry and Molecular Biology, University of Texas Medical Branch at Galveston, 301 University Boulevard, Galveston, TX 77555, USA
[9] Chemical and Biological Engineering Department, Montana State University, Bozeman, Montana, USA
[10] Département de Biochimie et Centre Robert-Cedergren en Bioinformatique et Génomique, Université de Montréal, Quebec, Canada
[11] Department of Emergency Medicine, Johns Hopkins Medicine, 5801 Smith Avenue, Suite 3220, Davis Building, Baltimore, MD, 21209, USA
[12] Department of Environmental Microbiology, Swiss Federal Institute of Aquatic Science and Technology (Eawag), 8600 Dübendorf, Switzerland.

[#]These authors contributed equally.
*Corresponding authors:
D.A.W. (weitz@seas.harvard.edu)
E.I.S. (shakhnovich@chemistry.harvard.edu)

ABSTRACT

Viral evolutionary pathways are determined by the fitness landscape, which maps viral genotype to fitness. However, a quantitative description of the landscape and the evolutionary forces on it remain elusive. Here, we apply a biophysical fitness model based on capsid folding stability and antibody binding affinity to predict the evolutionary pathway of norovirus escaping a neutralizing antibody. The model is validated by experimental evolution in bulk culture and in a drop-based microfluidics that propagates millions of independent small viral sub-populations. We demonstrate that along the axis of binding affinity, selection for escape variants and drift due to random mutations have the same direction, an atypical case in evolution. However, along folding stability, selection and drift are opposing forces whose balance is tuned by viral population size. Our results demonstrate that predictable epistatic tradeoffs between molecular traits of viral proteins shape viral evolution.

INTRODUCTION

The evolution of microbes and viral pathogens is affected by a hierarchy of constraints on multiple levels of biological organization (1). Mutations and other genetics changes primarily affect the structure and function of macromolecules, and these consequently change the fitness of the organism. Whether these arising mutations survive or are purged is also determined by the population size and dynamics. The first layer of constraints is defined by the relationship between mutations in the viral genome and the fitness of the individual virions (2). This relationship is the fitness landscape, which is a complex, multidimensional function; however, this can rarely be quantitatively determined. Nevertheless, it is essential for predicting selection of the most probable mutants. Several works have tried to quantitatively map organismal fitness to molecular properties. For example, bacterial fitness can be mapped to biophysical properties of core metabolic enzymes using flux-balance theory (3-7). Bloom and coworkers also demonstrated with Influenza that viral growth is strongly dependent on the folding stability of its nucleoprotein, which then constrains possible mutational pathways in its evolution (8). Recent experimental techniques that enable high-throughput and comprehensive interrogation of the fitness landscape, such as deep mutational scanning, confirm the pervasive role of folding stability in evolution (7, 9-15).

The second layer of constraint refers to how the fitness landscape itself is explored. The survival or purging of mutations in an evolving population is a function of competition, which is proportional to population size (16). In particular, population size changes the balance between the impact of random mutations on fitness and that of selection (17), and is thought to affect both the rate and direction of evolution (18). Recent studies have used microbial fitness landscapes (8, 19, 20) or population structure (21, 22) to predict the course of evolution, but to date, none links these elements together. Without this quantitative link between the biophysical phenotypes of the viral fitness landscape and the viral population demography, further progress in determining the course of viral evolution is significantly hindered.

In this paper, we quantitatively determine a biophysical fitness landscape for an RNA virus subjected to the pressure of a neutralizing antibody, and use it to account for the evolution of the

key biophysical traits of the viral antibody-binding epitope under conditions that constrain population size. The experimentally measured biophysical fitness landscape can be described by two biophysical parameters: the thermodynamics of folding of the capsid protein and its binding to the antibody. We probe the evolution of a model norovirus both in bulk, where population size is large, and in a microfluidic set-up that uses small drops to concurrently perform millions of evolution experiments (23-27) in very small population sizes. We show that the dynamics of viral adaptation is strongly dependent on population size. These results can be quantitatively described by a theoretical framework that combines protein biophysics and population genetics, providing the critical link between fitness landscape and population structure that enables exploring the quantitative interplay between the factors operating at different scales of biological organization—protein biophysics and viral population dynamics—in determining the course of viral evolution.

We focus in this work on Murine Norovirus (MNV), a model for human RNA viruses, which are a major cause of gastrointestinal disease epidemics in the world (28-30). MNV is a non-enveloped RNA virus that consists of 180 copies of the capsid protein assembled around a 7.5kb long positive-strand RNA genome. It mutates at ~1 base per genome per replication cycle and produces ~10^4 progenies in a single cell infection, of which ~100 are infectious viral particles, or plaque forming units (pfu) (23).

RESULTS

Lab evolution of Norovirus in large and small population sizes

To study viral evolution, we propagate a viral isolate (MNV-1, denoted as *wt*) in the presence of a neutralizing antibody (mAb6.2, (31)) that binds to the protruding domain (P-domain) of the capsid, and prevents viral entry into the host cell (32, 33). This set-up allows us to study the way the virus evolves to adapt to a new environment. To investigate the dynamics of this escape from the antibody, we sequence a 376 bp fragment of the genome encoding the epitope containing the outermost part of the P-domain (residues 281 – 412 of VP1) and follow the frequency of 37,244 unique haplotypes (see **Figure S1** for a schema of the approach and **Tables S1** and **Table S2** for

data) observed over several passages, allowing us to follow the evolution over several generations. First, we propagate *wt* in standard bulk culture conditions, using ~10^8 virions per passage under Ab pressure (**Figure 1A**). The population is initially dominated by the *wt* (~90% of the population) with the rest of the viral quasi-species consisting of single and double mutants (**Tables S1** and **S2**). After 2 passages the total number of surviving viruses has decreased by two orders of magnitude due to the neutralizing effect of the Ab (**Figure S2**); however, three single mutants E296K (*A*), D385G (*B*), T301I (*C*) as well as their double mutants (*AB*, *AC*, *BC*) occur at higher frequencies than the other haplotypes. By the fourth passage the triple mutant *ABC*, which first arises on passage 2, occurs at a frequency even higher than the other mutant haplotypes (86%); moreover, the total number of viruses increases to levels comparable to those observed after the first passage (**Figure S2C**). This suggests that *ABC* is an escape variant. Additionally, we note that the escape variant in bulk *ABC* is not present in the starting stock (**Table S1**), although some of the single- and double-mutants occur in the starting stock at low frequency. Thus, the escape variants arise from de novo mutations and not from standing genetic variation.

A central tenet of evolutionary theory is that the way organisms explore their fitness landscape depends on the size of their population, which controls the balance between random drift (i.e., direction of *randomly arising* mutations) in the population and positive selection (i.e., direction of beneficial mutations) (16, 17). This balance determines the most likely evolutionary pathways on a given fitness landscape. Indeed, the population size may be particularly important for noroviruses where a single viral particle is sufficient to infect the host animal (34); thus it is possible that viruses propagate in very small populations as they adapt to a new environment prior to the emergence of an epidemic. We can directly probe this hypothesis experimentally by drastically reducing population size compared to typical laboratory bulk cultures, which propagate ~10^6 to 10^8 viruses (**Figure S2C**). To evolve viruses in small population sizes we use a novel microfluidics set-up, which propagates ~10^6 subpopulations of 1-10 infectious particles (pfu) in distinct and non-mixing compartments (**Figure 2B**, **Figure S3**, **Movie S1** and **Movie S2**). The microfluidics system allows us to drastically reduce the population size without reducing the total number of viruses sampled, thereby maintaining the statistics comparable to that of a bulk experiment.

To ascertain that the effective population sizes between bulk and drops are indeed different, we measured the RNA titer (genomes/mL) in each passage, which fluctuates between 10^6 and 10^8 in bulk (**Figure S2 C, D**). Thus, a conservative estimate of the effective population size for the well-mixed bulk culture is $N_e=10^6$. On the other hand, the total number of viral genomes for all 10^6 drops ranges from 10^6 to 10^8, thus the average number of MNV-1 genome in a drop is 1 to 100. The effective population size in drops is therefore at least $N_e=1$ or at most $N_e=10^2$. Thus, the effective population sizes in drops and bulk differ by 4 to 6 orders of magnitude, which we estimate to be strong enough to give rise to different population dynamics.

In stark contrast with the bulk experiments, amplification and hence growth of potential escape variants that sweep the population is precluded when each variant is confined in a single drop with just two host cells; as a result, the *wt* remains the dominant fraction of the observed viruses through all passages. Potential escape viruses are present, but are in complete isolation from each other, at population sizes of just a single infection event per generation. This partitioning of single variants in the microfluidic setup (**Figure 1B, Figure 5D** and **Figure S3**) weakens selection and increases genetic drift as sub-populations evolve without competition between drops.

Next, we determine if the escapee is indeed more fit than the wild type. To address this question, we engineered the mutations *ABC* into the infectious clone and recovered mutant viruses. We then performed head-to-head competition of *wt* and *ABC* variants and show in **Figure 2** the frequency of each of the clones at the end of the competition. Indeed, *ABC* is a true escape variant since it outcompetes *wt* under neutralizing antibody. However, without antibody, *wt* is more fit than *ABC*, which explains the observation that *ABC* does not spontaneously arise in serial passaging without Ab.

Fitness landscape of norovirus escaping an antibody is projected onto the biophysical properties of its capsid domain

In general, fitness is expected to be a complex function of multiple traits. Instead we focus on the dependence of viral fitness in the presence of a neutralizing antibody on two biophysical properties of the epitope containing P-domain: The folding energy, which is a measure of stability, and the binding affinity to the antibody, which is a measure of neutralization. While the

importance of binding affinity to antibody is apparent, the universal importance of protein folding stability for bacterial and viral fitness was also shown (7, 8). This choice of variables is further supported by the fact that all the mutations of the dominant escape variants we observe in our experiments are located within the binding site between the P-domain and the Ab, as shown by mapping the mutations on the 3D structure of the *wt* P-domain in **Figure 3A**.

First, we calculate the folding energy of the P-domain and its binding affinity to the antibody for each haplotype sequence, using force field calculations based on the structural mapping in **Figure 3A** (35) to determine the change in folding energy $\Delta\Delta G_{fold}$ between the mutant and the *wt*; from this we determine ΔG_{fold} of the mutant by adding the folding energy of the *wt*, ΔG_{wt}. We also computationally determine the change in binding energy, $\Delta\Delta G_{bind}$, between the mutated P-domain-Ab complex and the *wt*; from this we determine the dissociation constant $K_d = K_0 \exp\left(\beta\Delta\Delta G_{bind}\right)$ where K_0 is the dissociation constant of the *wt*. We test the accuracy of our calculations by comparing the calculated biophysical properties of the escape haplotypes to experimentally measured properties. To accomplish this, we express and purify the P-domain of each haplotype and measure its binding to the Ab to extract K_d; we also measure the melting temperature of the P-domain, T_m, which correlates inversely to ΔG_{fold} (**Table S4** and ref. (36)). The measured values of the biophysical properties of the dominant escape haplotypes correlate strongly with the calculated values of the same haplotypes, as shown in **Figure 3B-C**. Importantly, we reverse engineer the escape viruses with their haplotype sequences on the background of the *wt* for the rest of the virus and confirm that the observed mutations in the P-domain are directly responsible for their increase in fitness both *in vitro* (**Figure 4A** and **Figure S6A**) and *in vivo* in mice (**Figure 4B** and **Figure S6B**); thus, our biophysical variables are relevant for viral fitness inside the real animal host.

The biophysical fitness landscape describes the dependence of viral fitness in the presence of a neutralizing antibody on ΔG_{fold} and $1/(mK_d)$, where the parameter m accounts for the multiple binding sites of the capsid. To arrive at a biophysical description of the viral fitness, we assume that the *wt* P-domain occurs in three specific states: folded and unbound, folded and bound, and unfolded (which is always unbound). The virus infects only when the P-domain is folded and unbound, hence, we can express the viral infectivity F at a given concentration of antibody $[Ab]$ as (37):

$$F = b_0 \frac{e^{-\beta \Delta G_{fold}}}{1 + e^{-\beta \Delta G_{fold}} + \frac{[Ab]}{mK_d} e^{-\beta \Delta G_{fold}}}, \qquad \textbf{(Equation 1)}$$

where the numerator is the Boltzmann factor describing the relative probability of being folded and unbound and the denominator is the partition function that sums over the probability of all three states, and $\beta=1/k_BT$ where k_B is the Boltzmann constant and T is the temperature. The function F has two regimes as shown by the surface in **Figure 3D**. For low binding affinities and stable P-domain structures, viruses are expected to infect host cells at some fixed probability, $0<b_0<1$, determined by the average effect of all remaining viral properties on the infection process, and $F=b_0$. By contrast, when the binding to the Ab is strong or when the P-domain is unstable, the virus cannot infect its host and $F=0$.

To compare the model to experiment, w e use sequencing data to determine the growth rate of each virus from the change in genome haplotype frequencies between successive generations (20). The growth rates distribute into two distinct groups with 87% of haplotypes exhibiting little or no growth and the rest exhibiting considerably larger growth. We take the first group to be non-infective, and take the second group to be infective (**Figure S4A**). For each haplotype sequence, we map the mutations to the 3D structure of the *wt* P-domain (35) and use force field calculations to determine the change in folding energy $\Delta\Delta G_{fold}$ between the mutant and the *wt*; from this we determine stability of the mutant $\Delta G_{fold}=\Delta G_{fold,wt}+\Delta\Delta G_{fold}$, where ΔG_{wt} is the folding energy of the *wt*. We also determine the change in binding energy, $\Delta\Delta G_{bind}$, between the mutated P-domain-Ab complex and the *wt*; from this we determine the dissociation constant $K_d=K_0e^{\beta\Delta\Delta G_{bind}}$ where K_0 is the dissociation constant of the *wt*. We bin the haplotypes using $\Delta\Delta G_{fold}$ and K_d and calculate F for each bin from the fraction of infective haplotypes. This binning exploits the large number of unique haplotypes to reduce the effects of errors in the calculations and of contributions from other biophysical properties. We fit the model by varying the three unknown parameters, b_0, ΔG_{wt} and the multiplier m.

We obtain excellent agreement between the model and the data, as shown by the dashed line in **Figure 3E-F**. The infectivity of haplotypes is zero at low K_d or high ΔG_{fold}, while at high K_d and low ΔG_{fold}, the landscape plateaus at F~0.25 independent of either of the biophysical coordinates.

The value of $1/m \approx 1.4\%$ obtained from the fit reflects the fact that only about 3 of the 180 P-domains on the capsid have to be blocked by the Ab to prevent infection (**Figure 3E** and ref. (23)). The value of $F \sim 0.25$ at the plateau is significantly less than the expected value of $b_0=1$; this points to the role of factors not included in the model, such as biophysical requirements for successful virus assembly and/or the interaction of the capsid with the host-cell receptor, in successful infection. In the absence of the neutralizing antibody, we do not expect the fitness landscape to depend on K_d, which is indeed the case (**Figure S5**). Altogether, these results demonstrate that binding and folding energies are very good predictors of viral extinction; however they are less successful in predicting infectivity. This suggests that antibody escape and folding stability of the capsid protein are necessary but not sufficient for viral infection.

We note that the parameter b_0, being the height of the sigmoidal function, reflects the optimal fitness when the viral capsid is both stable (negative ΔG) and free from the antibody (high K_d). That is b_0 is the fitness when the virus is on the plateau region of the landscape. The $\sim 10^4$ new virions in a single burst are, however, not uniformly distributed on the binding-stability plane (Figure **S4B**). In fact, most new virions fall in the unstable rather than stable regime in a ratio of approximately 100:1 (Figure **S4**), which recapitulates previous estimate that of the $\sim 10^4$ progenies in a single cell infection, ~100 are infectious viral particles, or plaque forming units (pfu) (23).

Population dynamics on the viral fitness landscape

We plot the position of viral haplotypes evolving on the landscape as a function of K_d and T_m and denote their allele frequencies by the size of the circles for each passage (see **Figure 5C,D** and **Table S4**). In the 5 independent bulk experiments, 4 evolved towards the fixation of variant *ABC* (represented also in Figure 1A) that has $T_m \sim 39.4$°C and $K_d \sim$ 23,300 nM and one lead to the fixation of variant *E* (L386F) that has $T_m \sim 45.0$°C and $K_d \sim$ 1,080 nM (**Table S4**). These two dominant variants that fixed in independent evolutionary runs manifest as two large circles in **Figure 5B**. Altogether, there is a clear trajectory as the intermediate variants evolve, having increasingly weaker affinities and higher T_m, with the escape variants at passage 5 ultimately having the weakest affinity, with an overall average of $K_d \sim$3,000 nM and the highest P-domain stability with an average of $T_m \sim 43.5$°C, as shown in **Figure 5B** (blue line).

We also plot the position of viral haplotypes evolving in ~1 million independent drop passaging experiments (**Figure 5C**), which shows that the predominant fraction of the population is wild type. The lack of clonal sweep is due to the fact that each lineage in the droplets is confined. For more quantitative comparison, shown in **Figure 5E,F** are the histograms of K_d and T_m in passage 5 of serial passaging only in bulk and in passage 5 of serial passaging only in drops. To ascertain that the population dynamics on the landscape under bulk and droplet conditions are distinct, we considered the ~10^6 independent serial passages of the droplet experiment as the null model. This large number of independent biological repeats achieved using the microfluidic setup provides statistical power. We estimate the likelihood of escape variants with T_m greater than or equal to T_m~39°C. This stability value is the threshold for the high fitness plateau of the landscape (**Fig. 5E**). Specifically, to estimate the probability of observing $T_m \geq 39$°C, we repeatedly draw 10^6 random variants from the null distribution, and then calculate this probability as the number of occurrences for variants with $T_m \geq 39$°C divided by 10^6. The resulting value of ~3×10^{-4} reflects the probability of observing an escape variant with $T_m \geq 39$°C in one experiment. Considering that the bulk escapee *ABC* (T_m=39.4°C) was observed in four out of 5 experiments and the escapee *E* (Tm=45.0°C) was observed in the remaining experiment, the overall probability of observing variants with $T_m \geq 39$°C in 5 independent experiments is ~2×10^{-18}.This analysis clearly indicates that higher folding stability of bulk escapee is the result of evolutionary selection rather than a random occurrence.

Balance between selection and random drift on the viral fitness landscape: Theory and Simulation

In general, the trajectories on the fitness landscape depend on the strength and direction of two evolutionary forces, drift and selection. To quantify the balance of these forces on the landscape, we use population genetics theory and calculate the ratio dN/dS, where *dN* is the rate of non-synonymous evolutionary rate and *dS* is the synonymous evolutionary rate (38) (For greater details, see section on Balance between selection and mutational drift on the fitness landscape in the Materials and Methods). Assuming that synonymous mutations are neutral, dN/dS =1 implies that non-synonymous mutations are also neutral because they are fixed at the same rate as synonymous mutations. Deviation from this expectation implies selection. Specifically, dN/dS >

1, implies positive selection for non-synonymous mutations, while dN/dS < 1 implies purifying selection.

We first limit ourselves to the simple case where a single mutation occurs on a monoclonal population, where the chance that the mutant eventually dominates is determined by its probability of fixation. To that end, we compare the probability of fixation of a non-synonymous mutation that changes folding stability and binding with the probability of fixation of a synonymous mutation, which we assume is neutral. We denote this ratio as ω. The underlying motivation for this ratio is that when ω=1, mutations are neutral at the level of fitness, and random drift dominates. Specifically, (39)

$$\omega = \frac{dN}{dS} = N_e P_{fix}\left(s, N_e\right) = N_e\left[\frac{1-\exp\left(-2s\right)}{1-\exp\left(-2N_e s\right)}\right] \qquad \textbf{(Equation 2)}$$

where $P_{fix}\left(s, N_e\right)$ is the probability of fixation (16) and N_e is the effective population size and s is the selection coefficient. The selection coefficient defines the fitness advantage of an arising mutation relative to wildtype, $s = \frac{F_{mut} - F_{wt}}{F_{wt}}$. Because we have a quantitative description of the fitness landscape (**Equation 1**), when a random mutation arises that changes the folding stability, $\Delta G_{fold} = \Delta G_{fold,wt} + \Delta\Delta G_{fold,}$ and the binding affinity $K_d = K_0 e^{\beta\Delta\Delta G_{bind}}$, the selection coefficient can be calculated explicitly (Methods for details):

$$\begin{aligned} s &= \frac{F_{mut} - F_{wt}}{F_{wt}} \\ &\approx \beta\Delta\Delta G_{bind}\frac{[Ab]}{mK_{d,wt}} - \beta\Delta\Delta G_{fold} e^{\left(\Delta G_{fold,wt}\right)} \end{aligned} \qquad \textbf{(Equation 3)}$$

The fitness (dis)advantage s is a function of the wildtype folding stability ΔG_{wt} and binding affinity K_0 and the changes induced by the mutation to folding stability and binding $\Delta\Delta G_{bind}$ and $\Delta\Delta G_{fold}$. This also implies that the dN/dS ratio is a function of the biophysical properties of the wildtype (ΔG_{wt} and binding affinity K_0), the changes induced by the mutation on folding and binding ($\Delta\Delta G_{fold}$ and $\Delta\Delta G_{bind}$, respectively), and effective population size.

The effect of random mutations on folding stability, denoted by the normalized probability density distribution $p(\Delta\Delta G_{fold})$, and on binding affinity, denoted by the normalized probability density distribution $p(\Delta\Delta G_{bind})$, are both well-characterized (40-42). Thus, we can derive the rate of protein evolution averaged over all possible effect of random mutations on folding and binding, that is,

$$\bar{\omega}\left(\Delta G_{fold}; K_{d,wt}; N_e\right) = \iint \omega p\left(\Delta\Delta G_{fold}\right) p\left(\Delta\Delta G_{bind}\right) d\left(\Delta\Delta G_{fold}\right) d\left(\Delta\Delta G_{bind}\right) \quad \textbf{(Equation 4)}$$

Eq. 4 defines the average stringency of selection as a function of background, and hence the strength of epistatic interaction on the fitness landscape defined by protein folding and binding. We show in **Figure 5A** (color map) the value of the integral over the range of $K_{d,wt}$ and $\Delta G_{fold,wt}$ values.

Indeed, positive selection is strongest when the *wt* P-domain is unstable (low ΔG) or tightly bound to the antibody. At large population sizes, purifying selection and positive selection dominates in the regime of low folding stability and tight binding affinity (red colors in **Figure 5A**). The prediction is that if the population starts in the unstable regime, it would migrate away from the regime where selection is strong and towards the regime where it is more neutral. In large population sizes, dN/dS exhibits a strong gradient towards high K_d and high folding stability (**Figure 5A**). Consequently, a *wt* population that is initially unstable and neutralized by Ab is expected to evolve resistance by increasing *both* K_d and stability. However, in small population sizes the gradient of dN/dS is directed only towards high K_d and the same initially unstable population will evolve resistance to Ab without increasing folding stability (**Figure 5B**).

The effect of population size on the course of evolution can be explained by analyzing the balance between selection and mutational drift, the two forces driving evolution. The direction of drift and selection along the trait of folding stability and binding affinity to the antibody can be inferred from protein engineering and systematic studies on effects of random mutations on proteins. Along the axis of folding stability ΔG_{fold}, beneficial mutations increase folding stability, but random de novo mutations in proteins tend to decrease stability(40-43). Thus, selection and drift act in opposite directions (**Figure 5A-B**, arrows), leading to mutation-selection balance.

Along the axis of binding affinity K_d, beneficial mutations for the virus lead to escape from Ab (towards high K_d), and random mutations on protein interfaces perturb binding (also towards high K_d). Thus, selection and drift act along the same direction (**Figure 5A-B**, arrows). We note that in general, and at the level of sequence space, the random genetic drift is indeed non-directional by definition. However, at the level of biophysical properties of proteins, there is directionality. Random mutations are predominantly destabilizing, thus drift points towards lower stability (Figure 5A,B). Random mutations are also predominantly perturbing the interfaces of PPI, thus drift points towards lower affinity (higher K_d).

For tractabilty, the theoretical analysis is done in the monoclonal regime, which holds only in the limit of weak mutation and strong selection(44), where mutations arise rarely and fix rapidly. This is not strictly applicable for an RNA virus like norovirus, which is polyclonal. Thus, to complement our theoretical analyses, we also simulate using a polyclonal viral population the trajectory for 4 sequential fixations of a single mutation starting from the position of the *wt* virus population on the viral fitness landscape (**Figure S7**; see also (37) for details). For large N, the simulations show that the norovirus population increases both its folding stability and dissociation constant, K_d, as it escapes the neutralizing antibody, following the trajectory shown by the solid points in **Figure 5A-B** (see also **Figure S7** for simulations in the polyclonal regime). After 4 sequential single mutations the model shows a rise of 5 orders of magnitude in K_d and an increase of 3kcal/mol in ΔG_{fold} towards stabilization corresponding to a change of 9°C in T_m. On the other hand, for small N the simulations show that the norovirus population increases its K_d to escape the antibody but exhibits only a small change in folding stability of less than 1 kcal/mol, corresponding to an increase in T_m of about 2°C, as shown by the trajectory in **Figure 5B** (see also **Figure 5A**).

Most likely pathways on the viral fitness landscape agree with predictions by protein biophysics and population genetics

We compare the theoretical prediction to the direction of evolution on the landscape in a bulk passaging that lead to *ABC* (**Figure 5C**). Indeed, the increase in K_d of the escapee in bulk *ABC* is accompanied by an increase in folding stability T_m=39.4°C (**Figure 5C, passage 5, red circle**). The other bulk escapee *E* has an even more dramatic increase in folding stability T_m=45.0°C

(shown in **Fig. 5C, passage 5, blue circle**). The variants *ABC* and *E* are bona fide escapees from the neutralizing antibody with K_d values that lead to the peak of the fitness landscape (**Figure 5E**). This result is supported by the head-to-head competition assays between WT and these variants in the presence and absence of antibody (**Figure 2**). Additionally, while the T_m values of the two bulk escapees *ABC* and *E* are different, they have comparable fitness because of the "plateau"-like or sigmoidal shape of the landscape.

In contrast, the viral mutants that propagate in drops increase in K_d while maintaining original T_m. In Passage 5 of the droplet experiment (**Figure 5D**), excluding the dominant *wt*, the other segregating variants have an average of K_d ~1,000 nM and T_m~38.3°C.

Strong epistasis and compensation among mutations that eventually lead to viral escape

There is epistasis on the fitness landscape as shown from the non-additive effect of the single mutations compared to the double- or triple-mutants. For example, the double mutants *AC, BC,* and *AB* have less than additive K_d showing negative epistasis (**Table S4**). This also holds for the folding stability. Based on simple biophysics, we can develop expectations on the (non)additive effect of mutations on K_d. The binding constant $K_d \sim \exp(\beta \Delta\Delta G_{\text{binding}})$, hence if two mutations *A* and *B* are non-interacting in the 3D structure (that is, non-epistatic), we can assume that they will have additive effect in the free energy of binding. Hence, for the ratio of the binding affinity of the double mutant to the binding affinity of the wildtype, $K_{d,AB}/K_{d,wt} = \exp(\beta \Delta\Delta G_{binding,\ mutant\ A} + \beta \Delta\Delta G_{binding,\ mutant\ B}) = (K_{d,A}/K_{d,wt})(K_{d,B}/K_{d,wt})$. Thus, under no epistasis, the *increase* in K_d of a double mutant is equal to the product of the increases on K_d of single mutants. The mathematical analog in evolutionary biology is the relationship Wright-Fisher fitness *w* and the Malthusian fitness *b*, which is $w \sim \exp(b)$. The absence of epistasis implied additive Malthusian fitness of multiplicative Wright-Fisher fitness. Indeed, the double- and triple-mutants have less than additive effect on K_d, which implies strong epistatic interactions among them (**Table S4**). These epistatic interactions have a structural basis because they are all found at the interface of the viral capsid-domain and the Fab domain of the neutralizing antibody. Notwithstanding the epistatic interactions among the mutations, in bulk, all single and double-mutants of the eventual escapee have all higher T_m and K_d compared to wildtype (**Figure 5**).

DISCUSSION

A key requirement in determining, and perhaps in our future ability in predicting, the evolutionary dynamics of viral and microbial pathogens is a quantitative description of their fitness landscape. This landscape, which is mapping of the full genotype-phenotype relationship, is complex. However, recent works have shown that in some biological and already very clinically relevant systems, such as evolution of bacterial resistance against antimicrobials (45) and evolution of viral resistance against antiviral treatments (8, 46), the fitness landscape may be quantitatively and systematically defined. Here, we have shown that the fitness landscape of a norovirus evolving against a neutralizing antibody is systematically described by the biophysical properties of its capsid domain, in particular, folding stability and binding affinity to the neutralizing antibody. These biophysical parameters are relevant to other viruses; for example, both binding (47) and folding stability (8) are relevant traits for the evolution of an influenza virus in the presence of a neutralizing antibody. Moreover, in this work, the dependence of fitness (viral infectivity) on these two traits is quantitatively predicted by theory based on the thermodynamics of protein folding and binding.

The geometry of the fitness landscape is strongly affected by population size (**Fig. 1**). In general, competition for limited resources (media or mammalian cells to infect) is function to the number of individuals; hence the strength of purifying selection and adaptive evolution is also proportional to population size. Specifically, we find that the fitness landscape is flatter when the viral population is evolved in deep-bottlenecked population size of ~100 virions in microfluidics. The flat landscape did not result in clonal sweeps. In contrast, standard bulk cultures where there were ~10^8 virions competing and the landscape is not flat, we observed multiple clonal sweep events. The escape variants showed the coupling between folding stability and binding—an increase in K_d to escape the neutralizing antibody is accompanied by an increase in folding stability. This coupling is not manifested in the flat landscape under low population size, as predicted by our simple biophysical model.

Projection of the fitness landscape on well-defined biophysical properties also enabled the quantification of the evolutionary forces on the landscape. As found by several groups, including ours (42, 48-50), the evolution of the folding stability as an evolutionary trait is determined by

the balance between selection for greater stability and mutational drift, which is predominantly destabilizing among random mutations (**Fig. 5**). This balance is tunable by population size because the magnitude of selection itself varies with population size (51, 52). The biophysical fitness landscape also allowed for the quantification of the evolutionary forces along the trait of binding affinity to the antibody. Unlike folding stability, the direction of selection (beneficial mutations) is in the same direction as random mutational drift (**Fig. 5**)—the supply of random mutations is predominantly biased towards perturbing the interface between the capsid and the antibody, and these same mutations are the most beneficial to viral escape. Thus, contrary to the classic notion that for a given trait, beneficial mutations are rare and evolution is the process of selection for these rare beneficial mutations, along the trait of binding affinity, beneficial mutations are in abundant supply. In essence, the evolutionary goal of the virus to escape against a neutralizing antibody is the opposite to the goals of enzyme design, which is to promote, instead of perturb, protein-protein interaction. To the best of our knowledge, this is the first definitive example in evolutionary biology, where selection and drift are in the same direction. However, we hypothesize that this may be ubiquitous and may also be found in evolution of antimicrobial resistance, where bacteria also want to escape an inhibitor. We note however, that in our experiments antibody itself did not evolve. The evolutionary force opposing pathogen escape– evolution of antibodies toward *higher* affinity to the antigen follow a more traditional intuitive scenario when selection and drift act in different directions (53).

Although binding affinity and folding stability of the MNV-1 capsid protein quantitatively map to infectivity, these two biophysical traits account for only ~30 % of infectivity (**Figure 3**). What might be the next most relevant axes of the viral fitness landscape? Protein dynamics and conformational flexibility is a strong candidate. For example, in MNV-1, it has been shown from structural studies of viral isolates that loop regions of their capsid sample multiple conformations, only some of which could bind to neutralizing antibodies (31).

We also found that the escape variant resistant to the neutralizing antibody is less fit in the absence of the antibody (**Fig. 2**). This suggests that there is a fitness cost to the evolution of resistance against the neutralizing antibody. The increase in frequency of intermediate escapees *B* and *AC* relative to the final escapee *ABC* in the absence of antibody (**Fig. 2, Passage 3,** -Ab) suggest that *ABC* might have higher fitness cost than either *B* or *AC*. More broadly, fitness cost

is well documented in the evolution of resistance against antibiotics(45, 54, 55). Although most resistant strains have a selective advantage in the presence of the antibiotic, they are often less fit in the absence of the drug. There is fitness cost associated with antimicrobial resistance because antibiotics target essential functions in the cell. Indeed, such is the case in our system—the neutralizing antibody targets the MNV-1 capsid's P-domain which is crucial for viral entry into the host cell(28).

Beyond the biophysical properties of the capsid proteins, viral fitness is also a function of replicative capacity inside the infected mammalian cell, the immune response of the host, and the fluctuations in effective concentration of neutralizing antibody. Altogether, combining our biophysical description of viral fitness landscape, together with these other factors, could lead to an integrative model of viral evolution.

MATERIALS AND METHODS

The materials and methods are described in detail within **SI Materials and Methods**. Briefly, to perform the lab evolution, we propagated a viral isolate (MNV-1) in the presence of a neutralizing antibody (mAb6.2, (31)) that binds to the protruding domain (P-domain) of the capsid, and prevents virus entry into the host cell (32, 33). And then, we deep sequenced using Illumina Miseq the 376 bp fragment of the genome encoding the outermost part of the P-domain (residues 281 – 412 of the VP1). We estimated the fitness (P_{infect}) of each haplotype based on its frequency throughout the passaging. We also estimated how the mutations in the haplotype change the folding stability of the P-domain of capsid and its binding affinity to the neutralizing antibody. These computational estimations of the biophysical properties were performed using the crystal structure of the proteins and a physical force field. We also purified the dominant clones, and then assayed their folding stability using thermal unfolding and binding affinity using surface plasmon resonance (SPR). The construction of the microfluidics devices for the serial passaging of the viruses in picoliter emulsions is described in the **SI Materials and Methods**.

ACKNOWLEDGEMENTS

The authors would like to acknowledge C. Wilke and J. Plotkin for very helpful comments. This work was supported by Defense Advanced Research Projects Agency (DARPA) contract # HR0011-11-C-0093, by the National Science Foundation (DMR-1310266 to DW and MCB-1243837 to ES), NIH GM068670 (ES), by the Harvard Materials Research Science and Engineering Center (DMR-1420570) and by the National Natural Science Foundation of China (HZ, 81372496).

COMPETING INTERESTS

The authors declare none.

REFERENCES

1. Bershtein S, Serohijos AW, & Shakhnovich EI (2017) Bridging the physical scales in evolutionary biology: from protein sequence space to fitness of organisms and populations. *Curr Opin Struct Biol* 42:31-40.

2. de Visser JA & Krug J (2014) Empirical fitness landscapes and the predictability of evolution. *Nat Rev Genet* 15(7):480-490.

3. Dykhuizen DE, Dean AM, & Hartl DL (1987) Metabolic flux and fitness. *Genetics* 115(1):25-31.

4. Flint HJ*, et al.* (1981) Control of the flux in the arginine pathway of Neurospora crassa. Modulations of enzyme activity and concentration. *Biochem J* 200(2):231-246.

5. Bershtein S*, et al.* (2015) Protein Homeostasis Imposes a Barrier on Functional Integration of Horizontally Transferred Genes in Bacteria. *PLoS genetics* 11(10):e1005612.

6. Bershtein S, Mu W, Serohijos AW, Zhou J, & Shakhnovich EI (2013) Protein Quality Control Acts on Folding Intermediates to Shape the Effects of Mutations on Organismal Fitness. *Molecular cell* 49(1):133-144.

7. Rodrigues JV*, et al.* (2016) Biophysical principles predict fitness landscapes of drug resistance. *Proc Natl Acad Sci U S A*.

8. Gong LI, Suchard MA, & Bloom JD (2013) Stability-mediated epistasis constrains the evolution of an influenza protein. *eLife* 2:e00631.

9. Fowler DM*, et al.* (2010) High-resolution mapping of protein sequence-function relationships. *Nat Methods* 7(9):741-746.

10. Bank C, Hietpas RT, Jensen JD, & Bolon DN (2015) A systematic survey of an intragenic epistatic landscape. *Mol Biol Evol* 32(1):229-238.

11. Jacquier H*, et al.* (2013) Capturing the mutational landscape of the beta-lactamase TEM-1. *Proceedings of the National Academy of Sciences of the United States of America* 110(32):13067-13072.

12. Sarkisyan KS*, et al.* (2016) Local fitness landscape of the green fluorescent protein. *Nature* 533(7603):397-401.

13. Firnberg E, Labonte JW, Gray JJ, & Ostermeier M (2014) A Comprehensive, High-Resolution Map of a Gene's Fitness Landscape. *Molecular biology and evolution* 31(6):1581-1592.

14. Baier F & Tokuriki N (2014) Connectivity between catalytic landscapes of the metallo-beta-lactamase superfamily. *J Mol Biol* 426(13):2442-2456.

15. Wrenbeck EE, Faber MS, & Whitehead TA (2016) Deep sequencing methods for protein engineering and design. *Current opinion in structural biology* 45:36-44.

16. Kimura M (1968) Evolutionary rate at the molecular level. *Nature* 217(5129):624-626.

17. Lynch M & Conery JS (2003) The origins of genome complexity. *Science* 302(5649):1401-1404.

18. Wright S (1931) Evolution in Mendelian Populations. *Genetics* 16(2):97-159.

19. Sanjuan R, Moya A, & Elena SF (2004) The distribution of fitness effects caused by single-nucleotide substitutions in an RNA virus. *Proceedings of the National Academy of Sciences of the United States of America* 101(22):8396-8401.

20. Acevedo A, Brodsky L, & Andino R (2014) Mutational and fitness landscapes of an RNA virus revealed through population sequencing. *Nature* 505(7485):686-690.

21. Lang GI*, et al.* (2013) Pervasive genetic hitchhiking and clonal interference in forty evolving yeast populations. *Nature* 500(7464):571-574.

22. Nahum JR*, et al.* (2015) A tortoise-hare pattern seen in adapting structured and unstructured populations suggests a rugged fitness landscape in bacteria. *Proc Natl Acad Sci U S A* 112(24):7530-7535.

23. Fischer AE*, et al.* (2015) A high-throughput drop microfluidic system for virus culture and analysis. *Journal of virological methods* 213:111-117.

24. Guo MT, Rotem A, Heyman JA, & Weitz DA (2012) Droplet microfluidics for high-throughput biological assays. *Lab Chip* 12(12):2146-2155.

25. Tao Y*, et al.* (2015) Rapid, targeted and culture-free viral infectivity assay in drop-based microfluidics. *Lab on a chip* 15(19):3934-3940.

26. Tao Y*, et al.* (2015) Artifact-free Quantification and Sequencing of Rare Recombinant Viruses Using Drop-based microfluidics. *Chembiochem : a European journal of chemical biology*.

27. Zhang H*, et al.* (2015) Isolation and Analysis of Rare Norovirus Recombinants from Coinfected Mice Using Drop-Based Microfluidics. *J Virol* 89(15):7722-7734.

28. Wobus CE, Thackray LB, & Virgin HWt (2006) Murine norovirus: a model system to study norovirus biology and pathogenesis. *J Virol* 80(11):5104-5112.

29. Ettayebi K*, et al.* (2016) Replication of human noroviruses in stem cell-derived human enteroids. *Science* 353(6306):1387-1393.

30. Jones MK*, et al.* (2014) Enteric bacteria promote human and mouse norovirus infection of B cells. *Science* 346(6210):755-759.

31. Kolawole AO*, et al.* (2014) Flexibility in Surface-Exposed Loops in a Virus Capsid Mediates Escape from Antibody Neutralization. *Journal of virology* 88(8):4543-4557.

32. Taube S*, et al.* (2010) High-resolution x-ray structure and functional analysis of the murine norovirus 1 capsid protein protruding domain. *J Virol* 84(11):5695-5705.

33. Katpally U, Wobus CE, Dryden K, Virgin HWt, & Smith TJ (2008) Structure of antibody-neutralized murine norovirus and unexpected differences from viruslike particles. *J Virol* 82(5):2079-2088.

34. Teunis PF*, et al.* (2008) Norwalk virus: how infectious is it? *Journal of medical virology* 80(8):1468-1476.

35. Yin S, Ding F, & Dokholyan NV (2007) Eris: an automated estimator of protein stability. *Nature methods* 4(6):466-467.

36. Privalov PL (1979) Stability of proteins: small globular proteins. *Adv Protein Chem* 33:167-241.

37. Cheron N, Serohijos AW, Choi JM, & Shakhnovich EI (2016) Evolutionary dynamics of viral escape under antibodies stress: A biophysical model. *Protein Sci* 25(7):1332-1340.

38. Yang Z & Nielsen R (2002) Codon-substitution models for detecting molecular adaptation at individual sites along specific lineages. *Mol Biol Evol* 19(6):908-917.

39. Nielsen R & Yang Z (2003) Estimating the distribution of selection coefficients from phylogenetic data with applications to mitochondrial and viral DNA. *Molecular biology and evolution* 20(8):1231-1239.

40. Tokuriki N, Stricher F, Schymkowitz J, Serrano L, & Tawfik DS (2007) The stability effects of protein mutations appear to be universally distributed. *J Mol Biol* 369(5):1318-1332.

41. Moal IH & Fernandez-Recio J (2012) SKEMPI: a Structural Kinetic and Energetic database of Mutant Protein Interactions and its use in empirical models. *Bioinformatics* 28(20):2600-2607.

42. Zeldovich KB, Chen P, & Shakhnovich EI (2007) Protein stability imposes limits on organism complexity and speed of molecular evolution. *Proc Natl Acad Sci U S A* 104(41):16152-16157.

43. Kumar MD*, et al.* (2006) ProTherm and ProNIT: thermodynamic databases for proteins and protein-nucleic acid interactions. *Nucleic acids research* 34(Database issue):D204-206.

44. Kryazhimskiy S & Plotkin JB (2008) The population genetics of dN/dS. *PLoS genetics* 4(12):e1000304.

45. Rodrigues JV*, et al.* (2016) Biophysical principles predict fitness landscapes of drug resistance. *Proceedings of the National Academy of Sciences of the United States of America* 113(11):E1470-1478.

46. Cheron N, Serohijos AWR, Choi JM, & Shakhnovich EI (2016) Evolutionary dynamics of viral escape under antibodies stress: A biophysical model. *Protein Sci* 25(7):1332-1340.

47. Fonville JM*, et al.* (2014) Antibody landscapes after influenza virus infection or vaccination. *Science* 346(6212):996-1000.

48. Bloom JD*, et al.* (2005) Thermodynamic prediction of protein neutrality. *Proceedings of the National Academy of Sciences of the United States of America* 102(3):606-611.

49. Bloom JD, Raval A, & Wilke CO (2007) Thermodynamics of neutral protein evolution. *Genetics* 175(1):255-266.

50. Serohijos AW & Shakhnovich EI (2014) Merging molecular mechanism and evolution: theory and computation at the interface of biophysics and evolutionary population genetics. *Current opinion in structural biology* 26:84-91.

51. Serohijos AW, Lee SY, & Shakhnovich EI (2013) Highly abundant proteins favor more stable 3D structures in yeast. *Biophys J* 104(3):L1-3.

52. Wylie CS & Shakhnovich EI (2011) A biophysical protein folding model accounts for most mutational fitness effects in viruses. *Proc Natl Acad Sci U S A* 108(24):9916-9921.

53. Zhang J & Shakhnovich EI (2010) Optimality of mutation and selection in germinal centers. *PLoS computational biology* 6(6):e1000800.

54. Andersson DI & Hughes D (2010) Antibiotic resistance and its cost: is it possible to reverse resistance? *Nature reviews. Microbiology* 8(4):260-271.

55. Sousa A, Magalhaes S, & Gordo I (2012) Cost of antibiotic resistance and the geometry of adaptation. *Molecular biology and evolution* 29(5):1417-1428.

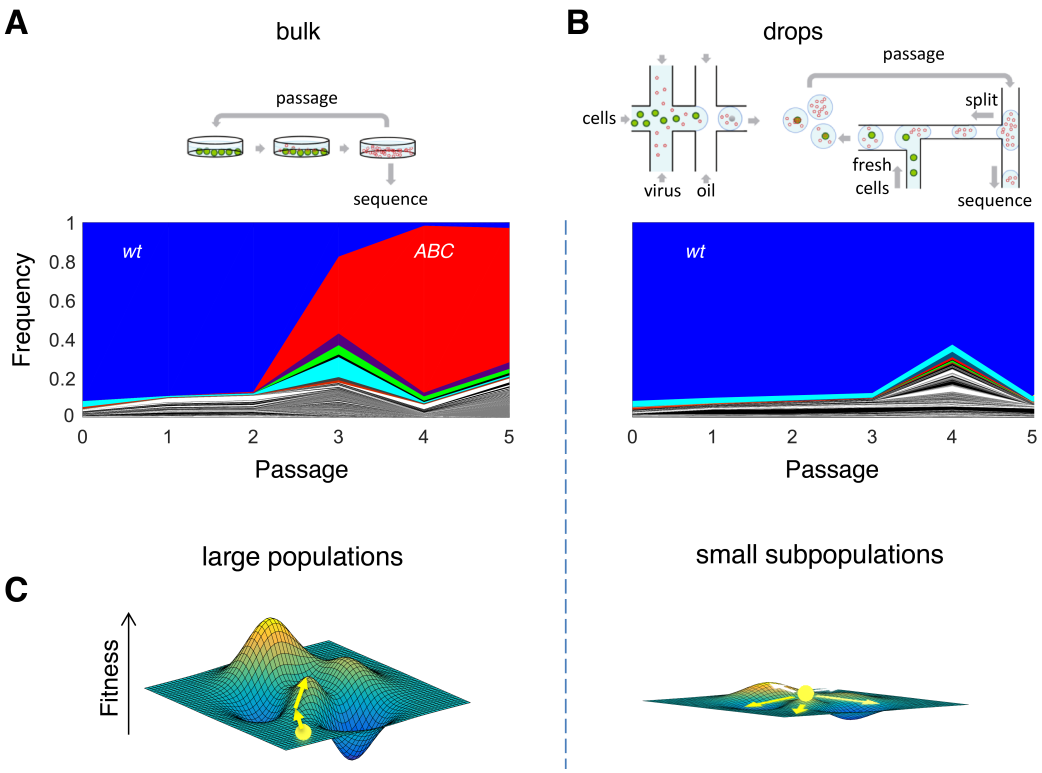

Figure 1. Viral evolution in large and small population sizes.

A) Viral evolution in large populations. Top: 10^8 viruses evolving against a neutralizing antibody by serial propagation in bulk. **Bottom:** The allele frequencies of 1,364 distinct P-domain haplotype sequences are plotted per passage (**Figure S2A,B**). **B) Viral evolution in small populations.** 10^6 pico-liter drops are loaded with on average 1 virus and 2 host cells per drop and the viruses evolve in drops for five passages (see also **Figure S3** and **Movie S1, S2**). **C)** The perceived ruggedness of the fitness landscape depends on the population size. Haplotype legend: A: E296K, B: D385G, C: T301I, D: A382V.

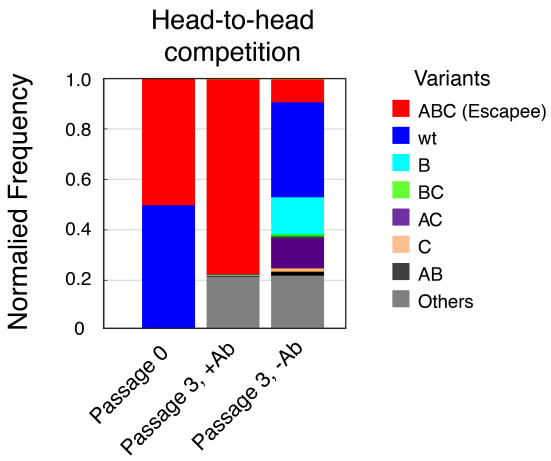

Figure 2. Head-to-head competition between wildtype and escapee

To perform pairwise competition of the clones, we mixed equal titers of the clone, propagate them for 3 passages, and then perform deep sequencing. Averages over 3 biological replicates are shown for each measurement. See also Table S3.

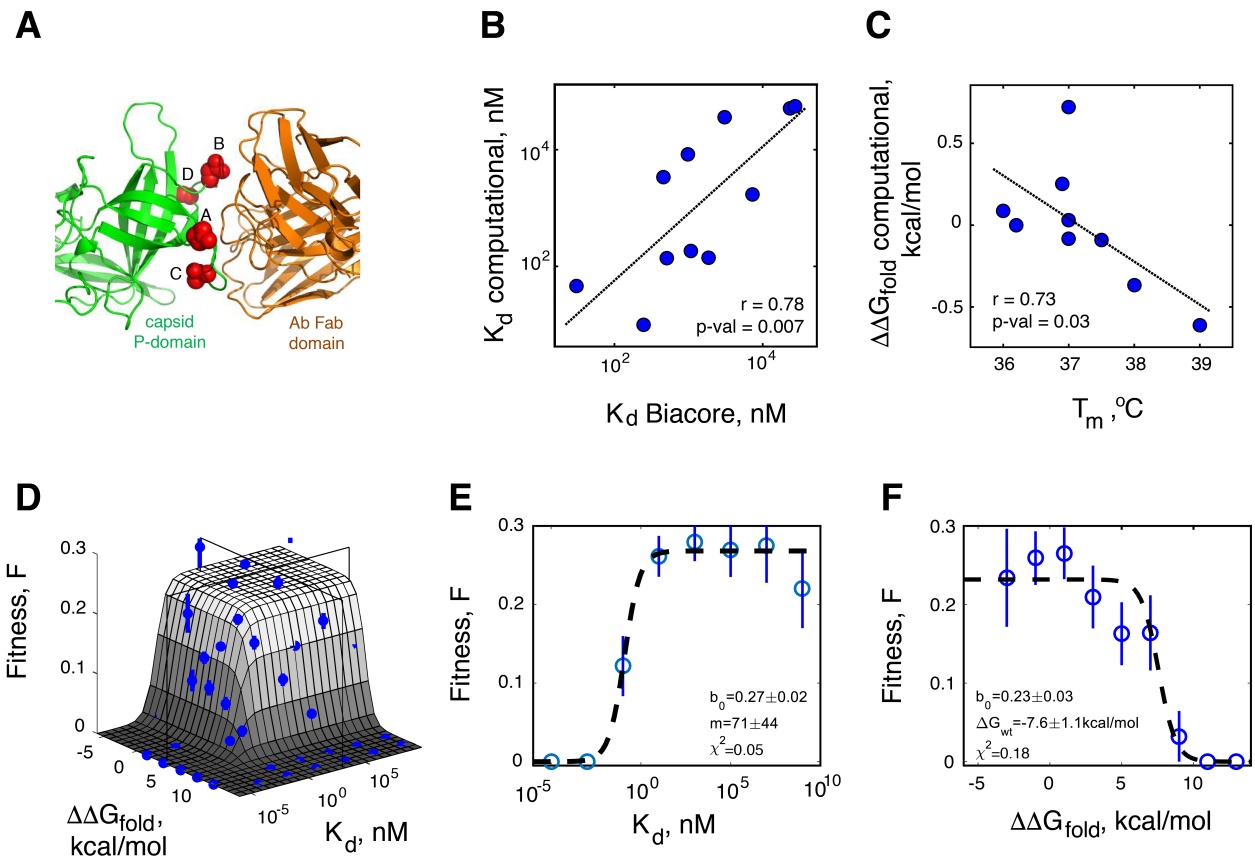

Figure 3. Fitness landscape of norovirus escaping a neutralizing antibody

A) The P-domain Antibody complex structure. The SNPs of all dominant P-domain variants (red circles) are located on the docking site of the P-domain-antibody complex (PDB ID: 3LQE). **B)** A high correlation exists between Ab dissociation constant K_d that was experimentally measured using surface plasmon resonance (SPR) and the one computed from force field calculations. **C)** The anti-correlation between the experimentally measured P-Domain melting temperature (T_m) and the folding stability computed from force field calculations. Two outlier variants were excluded from the analysis. **D)** A 3D plot of the probability of infection F averaged over 2,076 distinct haplotypes binned according to their dissociation constant K_d and folding stability ΔG_{fold} (blue points) overlaid with the theoretical fit according to Equation 1 (gray surface). Cross sections (black frames) demark the regions used for the projections in E and F. **E)** The probability of infection for all haplotypes with ΔG_{fold}<4.5Kcal/mol (cross section parallel to K_d axis in A) is projected on the K_d-F plane, binned according to their K_d (blue points) and overlaid with the theoretical fit to Eq. 1 (dashed line). **F)** The probability of infection for all haplotypes with K_d>10^3nM (cross section parallel to ΔG_{fold} axis in A is projected on the ΔG_{fold}-F plane, binned according to their ΔG_{fold} (blue points) and overlaid with the theoretical fit to **Equation 1** (dashed line). F is determined from deep sequencing lysates of *in vitro* experiments in the presence of neutralizing antibody. K_d and ΔG_{fold} are estimated from mapping the haplotype mutations to the 3D structure of the capsid P-domain in complex with the neutralizing antibody. Error bars in panels D, E and F denote Standard Error.

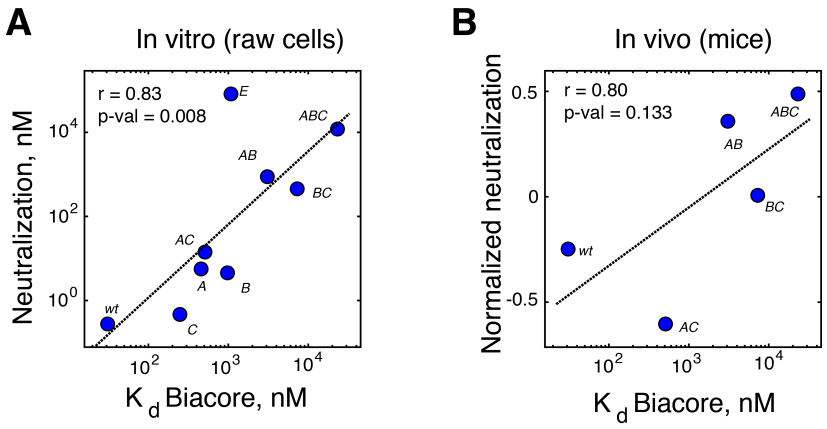

Figure 4. MNV-1 neutralization versus binding affinity of the P-domain to neutralizing antibody.

A) *In vitro* neutralization of dominant haplotypes correlates to their K_d and the average ratio between them is ~120, in good agreement with the modeled value of $m \approx 70$ (see **Figure 3E** and **Equation 1**) (Supplementary Methods: In-vitro neutralization measurements). **B)** *In vivo* neutralization of dominant haplotypes in mice correlates to their K_d. Viral strains were neutralized in STAT-/- mice injected with 500ug mAb A6.2 and compared to their infection in mice injected with an isotype as described in (13). The decrease in viral titers was first standardized for each tissue across viral strains, before the average over all tissues within each strain was taken as its final neutralization score.

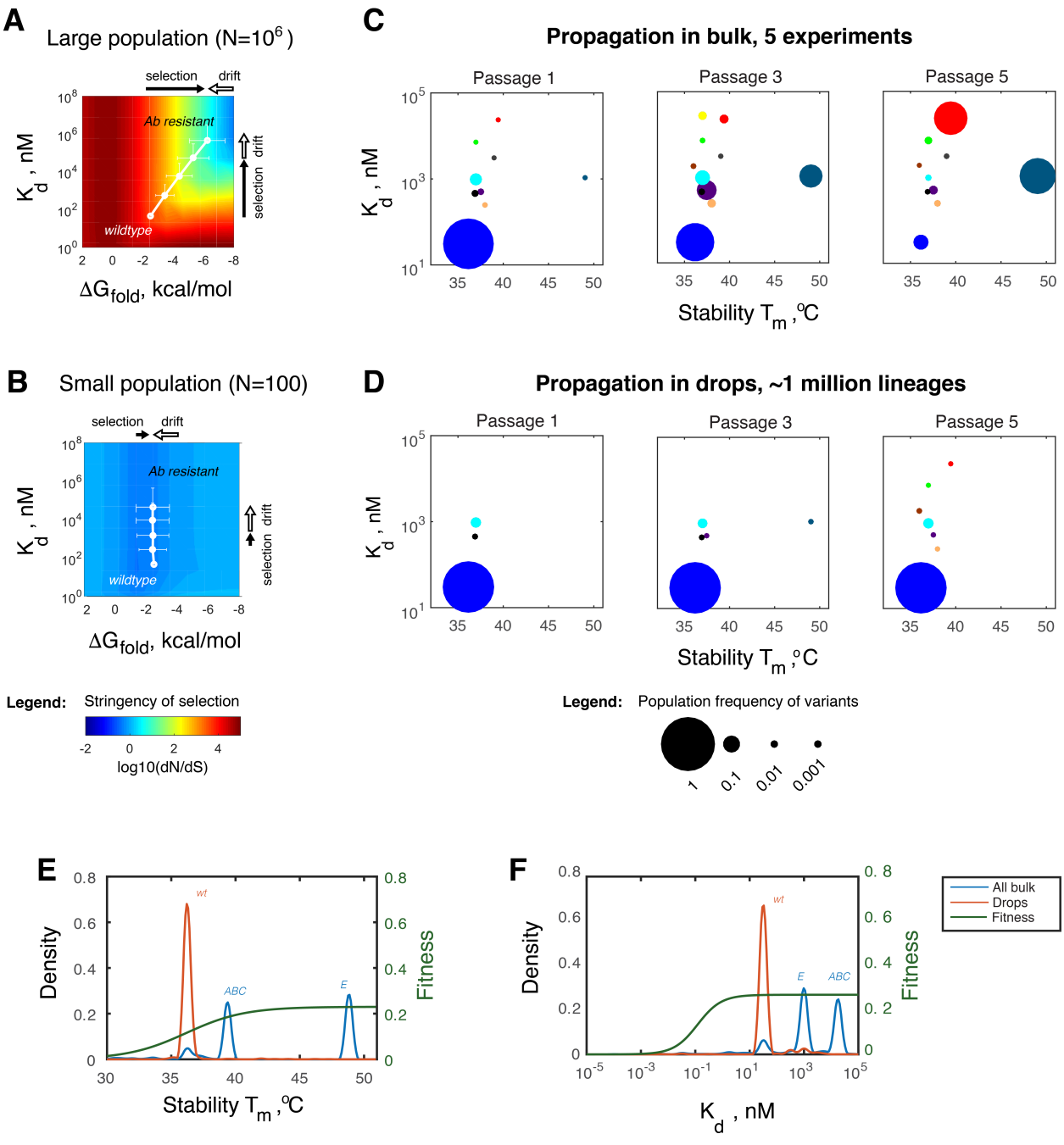

Figure 5. Dominant haplotypes from bulk and droplet experiments.

A and B) Average stringency of selection for several population sizes (see Text). For large population sizes, the increase in K_d is strongly coupled to the increase in T_m. However, for small population sizes, the selection for K_d is decoupled from the selection for folding stability. The white lines are the predicted trajectories from forward evolutionary simulations of an MNV population escaping an Ab, but with a P-domain that is unstable. Each trajectory is the average of 1000 independent simulations. The direction of selection (black arrows) is towards greater folding stability and weaker affinity to the antibody. Selection is strong when the P-domain is

unstable and/or is tightly bound to the Ab. Selection pressure is approximately zero when the fitness landscape is flat (neutral). Along the direction of folding stability, most random mutations are destabilizing which lead to a random drift (white arrows) towards protein destabilization. Along binding affinity axis, most random mutations perturb the protein-protein interaction that leads to a random drift towards weaker binding. **C and D)** Density plots of all haplotypes grouped according to passages. Biophysical properties were measured and their size represents the allele frequency of each haplotype, see also legend inset. **E and F**). Histograms of K_d and T_m in passage 5 of serial passaging only in bulk and in passage 8 of the bulk expansion after rounds of evolution in drops. The positions of the escape variants are shown in the projection of the fitness landscape (green line, see also **Figure 3E,F**). The variants *ABC* and *E* are bona fide escapees from the neutralizing antibody with K_d values that lead to the peak of the fitness landscape. Although the T_m values of the two bulk escapees *ABC* and *E* are different, they have comparable fitness because of the "mesa"-like nature of the landscape. To ascertain that the population dynamics on the landscape under bulk and droplet conditions are distinct, we considered the $\sim 10^6$ independent serial passages of the droplet experiment as the null model. We estimate the likelihood of escape variants with T_m greater than or equal to $T_m \sim 39°C$. This stability value is the threshold for the high fitness plateau of the landscape (**Fig. 6E**). Specifically, to estimate the probability of observing an escapee with $T_m \geq 39°C$, we repeatedly draw 10^6 random variants from the null distribution, and then calculate this probability as the number of occurrences for variants with $T_m \geq 39°C$ divided by 10^6. The resulting value of $\sim 3 \times 10^{-4}$ reflects the probability of observing a bulk escapee with $T_m \geq 39°C$ in one experiment. The overall probability of observing variants with $T_m \geq 39°C$ in 5 independent experiments is $\sim 2 \times 10^{-18}$.